Compact Fluorescence Detection System Based on a Monolithic DBR-Integrated III-Nitride LED Chip

Jiabin Yan,*,† Jianwei Fu,† Fan Shi,† Xumin Gao,* Feifei Qin, Pengzhan Liu, and Yongjin Wang*

ACCESS | Metrics & More | Article Recommendations | Supporting Information

ABSTRACT: Portable applications of fluorescence detection systems have gained much attention in various fields and require system components to be small and compact. In this work, we report on a compact fluorescence detection system and demonstrate its application for fluorescence sensing and imaging. The light source and filter are integrated on a single chip for the proposed system, which not only realizes the separation between excitation and fluorescent lights but also improves the light-emitting diode (LED) light extraction efficiency. Furthermore, the detection system allows for a removable sample unit. The results indicate that the performance of the distributed Bragg reflector (DBR) filter based on an amorphous dielectric film is excellent with selection ratios larger than 4600:1. The peak emission wavelength of the LED is 528 nm. The influence of green light leakage can be neglected, and the fluorescent red light is dominant when the fluorescence detection system is used for sensing and imaging. The low-cost and monolithic DBR-integrated III-nitride LED chip makes the proposed architecture a competitive candidate for portable fluorescence detection applications.
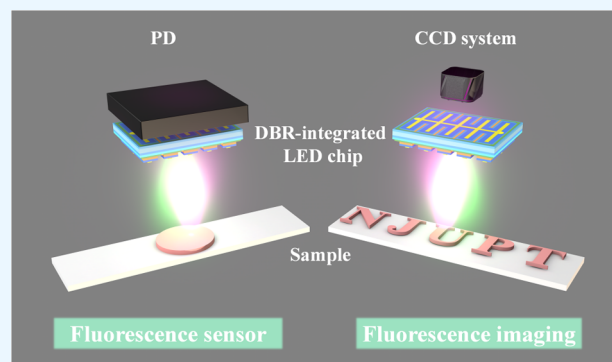
1. INTRODUCTION

Fluorescence detection is one of the most widely used techniques for living cell/tissue imaging and antigen/antibody identification in bioresearch and medical diagnosis,[1−6] determination of specified ions or gas in environmental monitoring,[7−12] and even strain/ temperature measurement.[13] A typical fluorescence sensor system mainly consists of an excitation light source, one or more filters, a photo-detector (PD), and fluorescent samples.[14,15] When the excitation light illuminates the fluorescent samples, the intensity or phase of the fluorescent light indicates the physical parameters of the target.[16] Through the PD, the fluorescent light is converted into an electric signal, and this information is easily processed and analyzed. Similar to the sensor system, a fluorescence imaging system can be constructed just by replacing the PD with an imaging device such as a charge-coupled device (CCD). For the sensor or imaging system, the excitation light source can be a laser diode (LD) or a light-emitting diode (LED), and the filters are used to separate the excitation light and fluorescent light. Besides the commonly used filters, sample preparation using long-lasting phosphorescent materials can also realize the light separation because the excitation light illumination and fluorescent light detection are performed at different times.[17,18] However, the sample characteristics greatly limit the application of long-lasting phosphorescent materials used in a practical fluorescence detection system. The filter-based fluorescence sensor system remains the most common, and the performance of the filter is a key factor to improve the system detectivity. Available technologies include interference filters, absorption filters, and polarizing filters.[19] The interference filters based on an amorphous dielectric film with a distributed Bragg reflector (DBR) structure are preferred for high-performance sensor systems because of their excellent selectivity.

The multicomponent integration based on micro- and nanofabrication technologies has a tremendous impact on the development of fluorescence detection.[20,21] First, the size and weight can be greatly reduced by replacing the traditional bulky and discrete elements with chip-scale integrated ones which are more compact and reliable. The size and weight reductions are beneficial for portable applications and on-site testing. Second, as the chip-scale integrated components in the detection system allow for mass production, the costs of the detection system can be greatly reduced. For example, Thrush et al. have proposed a low-cost, compact, and parallel architectured semiconductor fluorescence sensor which integrates a vertical-cavity surface-emitting LD, a PIN PD, and an optical emission filter.[21] However, the sensor sensitivity was

limited by the laser background due to direct light coupling through device sidewalls and the relative poor performance of the filter.

With the advantages of low power consumption, a long lifetime, high reliability, a compact structure, and so on,[22−24] the III-nitride multiple quantum well (MQW) LED has gained extensive attention in various applications[25−28] and is an ideal excitation light source for the fluorescence detection system. Therefore, we propose a compact fluorescence detection system based on a monolithic DBR-integrated III-nitride LED chip in this work. The application of the proposed detection system for fluorescence sensing and imaging has been successfully demonstrated. A DBR filter directly covers the backside of the sapphire substrate of the uniformly luminous LED, which results in the improvement of LED light extraction efficiency and effective separation of excitation and fluorescent lights. Because the excitation light source and the PD/CCD are placed on the same side of the fluorescent sample for the proposed system, this scheme allows for a removable sample unit, and the requirements for sample preparation are much lower. Moreover, the PD of the sensor system can be easily replaced by an optical fiber connector for spectral analysis. The sensor device and system design are presented in Section 2. Section 3 provides the experimental results and related discussion.

2. DESIGN AND FABRICATION

The III-nitride MQW LEDs are fabricated through a wafer-scale micro-fabrication process. The epitaxial layers of the LED wafer, which are grown on a 4 in. c-plane sapphire substrate by metal−organic chemical vapor deposition, contain an unintentionally doped gallium nitride (u-GaN) layer, an n-doped GaN layer, an $In_{0.25}Ga_{0.75}N/GaN$ MQW layer (400 nm), and a p-doped GaN layer, with a total thickness of 6 μm. As illustrated in Figure 1a, four major fabrication steps can realize the
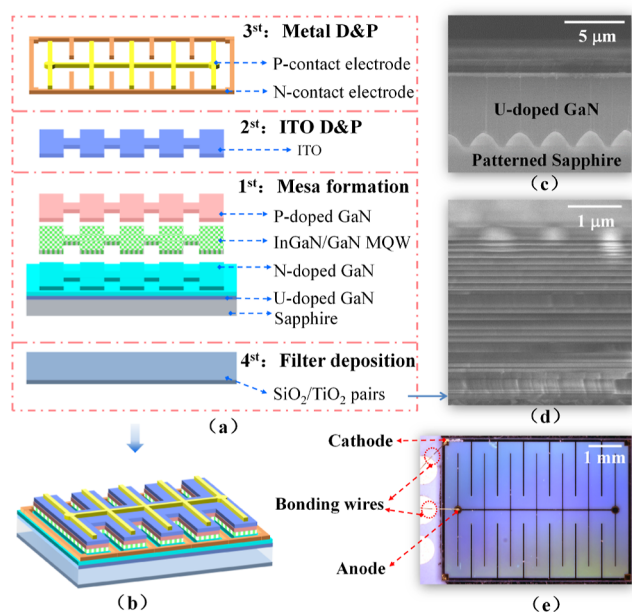

Figure 1. (a) Layer structure of the proposed III-nitride MQW LED and major fabrication steps. (b) Schematic overview of the LED. (c) SEM cross-sectional image of the epitaxial layers. (d) Cross-sectional view of the interference filter. (e) Optical microscopy image of the LED.

structure of the proposed monolithic DBR-integrated III-nitride LED chip shown in Figure 1b. First, using photoresist as a mask, inductively coupled plasma (ICP) etching is performed with a mixture of Cl_2 and BCl_3 to form the mesas as light-emitting regions. The regions without the protection of the photoresist are etched to the n-doped GaN layer. Second, a transparent indium tin oxide (ITO) current-spreading layer with a thickness of 230 nm is deposited by sputtering and treated by rapid thermal annealing subsequently at 530 °C in a N_2 atmosphere for 7 min to improve the electrical properties. Then, the ITO layer is patterned by lithography and ICP with a mixture of $HCl/FeCl_3$. Third, the P-contact and N-contact electrodes (Ni/Al/Ti/Pt/Ti/Pt/Au) are deposited by electron beam evaporation and patterned by lift-off process, followed by rapid thermal annealing at 850 °C in a N_2 atmosphere for 30 s. Fourth, after thinning the sapphire substrate down to 200 μm, an interference filter containing 50 SiO_2/TiO_2 pairs is deposited on the backside of the sapphire substrate. Finally, the separate LED chips with the size of 5.6 cm × 4.3 cm are obtained by wafer dicing using ultraviolet nanosecond laser micromachining. Figure 1c shows the scanning electron microscope cross-sectional image of the epitaxial layers of the LED wafer. The patterned sapphire substrate is adopted to improve the crystalline quality of epitaxial layers.

Figure 1d shows the cross-sectional view of the interference filter. For reflecting the excitation blue light and letting the fluorescent light through, the filter with DBR structure needs careful design and can be flexibly adjusted according to the properties of the fluorescent sample. The detailed structure parameter shown in Figure 2a is obtained by theoretical calculation using thin-film theory and transfer matrix algorithm. Figure 2b presents the contrast in result between theoretical calculation and measurement. It can be seen that the calculated result is in good agreement with the measured result. The transmission decreases sharply with wavelength from 605 to 590 nm. The measured transmission is larger than 92% with wavelength from 615 to 800 nm and less than 0.02% with wavelength from 420 to 575 nm. Compared to the calculated transmission larger than 99.9% with wavelength from 615 to 800 nm, the measured transmission has a certain constant loss. The reason is due to the interface reflection at the top side of the LED chip. For the fluorescence detection application, the selection ratio of the integrated DBR filter is excellent (larger than 4600:1), which is beneficial for reducing the difficulty of optical signal processing.

3. RESULTS AND DISCUSSION

First, the luminescence performance of the III-nitride MQW LEDs is characterized using an integrating sphere (Labsphere 3P-GPS-053-SL) with a calibrated detector under continuous wave pumping conditions. The measured external quantum efficiencies (EQEs) and radiation fluxes with respect to injected current are presented in Figure 3a. The EQEs increase from a low value (2.98% for LED with DBR and 1.53% for LED without DBR) at 10 mA to peak values (13.02% for LED with DBR and 8.06% for LED without DBR) at 340 mA and drop slowly at a larger current. The EQE and radiation flux of the LED integrated with a DBR filter is obviously higher than that without DBR. The reason is that the light reflected by the DBR filter contributes to the radiation flux. In contrast, the emitted light goes through the sapphire substrate and is partly absorbed by the printed circuit board (PCB) packaging for the LED without DBR. Figure 3b shows the electroluminescence
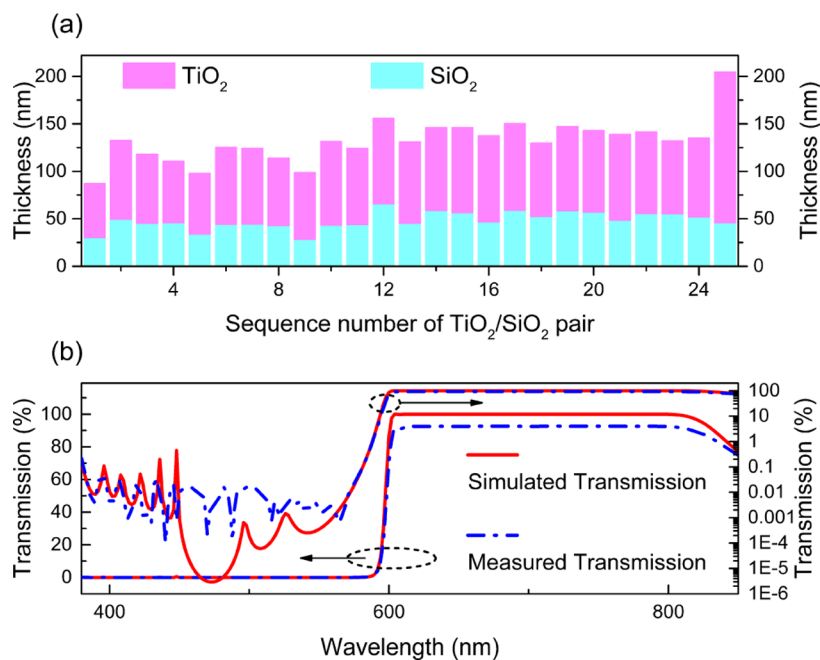
Figure 2. (a) Detailed structure parameter of the DBR filter. (b) Measured and simulated transmission of the fabricated DBR filter.
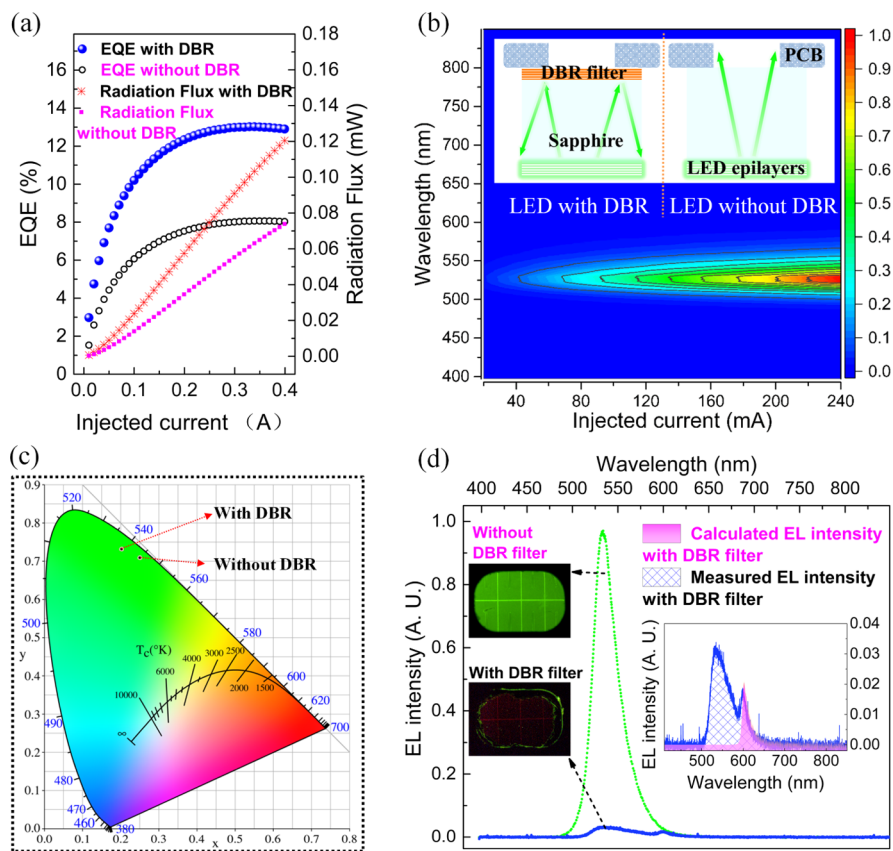

Figure 3. (a) Measured EQEs and radiation fluxes with respect to the injection current. (b) EL spectra versus the injection current of the device without the DBR filter. Inset shows the schematics of the packaged LED chips with and without the DBR filter in the test. (c) Coordinates in CIE 1931 chromaticity diagram for LEDs with and without the integrated DBR filter under an injection current of 400 mA. (d) EL spectra detected at the backside of LED chips with and without the DBR filter. Left insets show the backside optical microscopy images of LEDs and the right inset compares the calculated and measured EL intensities with the DBR filter.

(EL) spectra versus the injected current of the device. The emission intensity increases with the injected current and the peak wavelength is stable at 528 nm. Figure 3c marks the

coordinates of (0.2024, 0.7319) and (0.2502, 0.71) in the Commission Internationale de l'Eclairage (CIE) 1931 chromaticity diagram for LEDs with and without an integrated
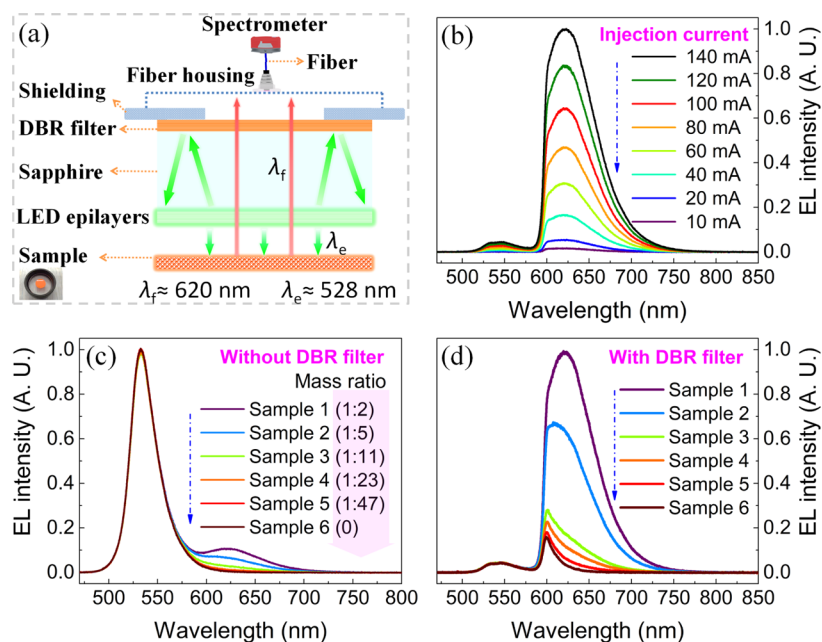
Figure 4. (a) Measurement setup for spectral analysis of the fluorescence detection system. (b) Normalized EL intensity of the system with the DBR-integrated LED and fluorescent sample 1. (c) Normalized EL intensity of the fluorescence detection system for different fluorescent samples using an LED without the DBR filter. (d) Normalized EL intensity of the fluorescence detection system for different fluorescent samples using an LED with the DBR filter.
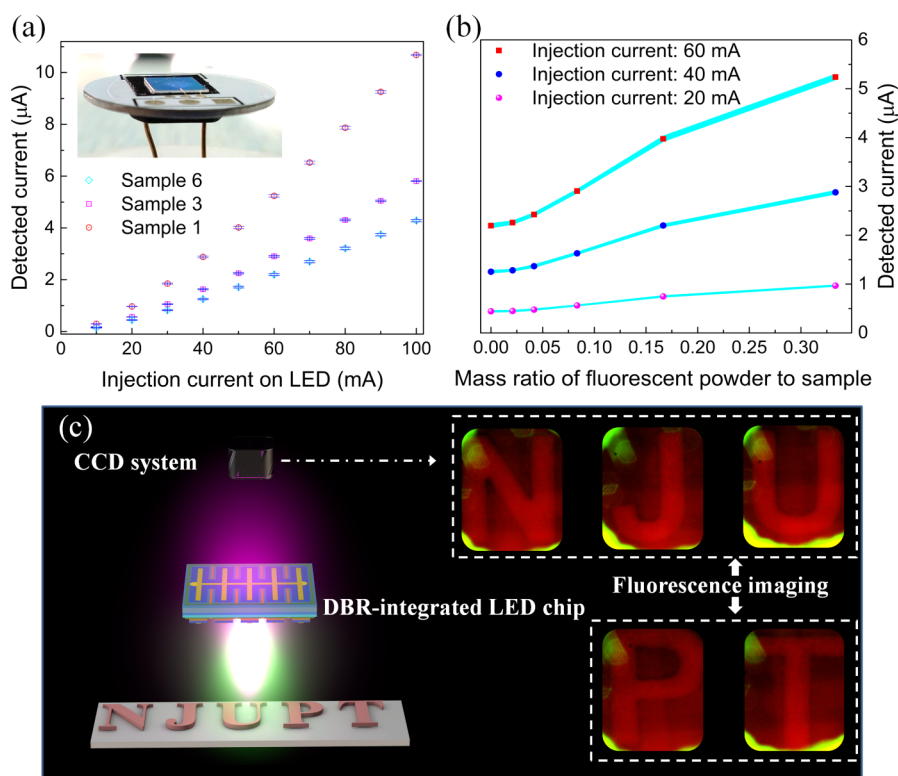

Figure 5. (a) Detected PD current with respect to the injected current on the LED. Inset shows the packaged fluorescence sensor image. The scattered data symbols denote the average value of four repeated measurements, and the errors bars show the deviations. (b) Detected PD current with respect to the mass ratio of fluorescent powder to the sample. The error bars are in line style, and the thickness indicates the standard deviation. (c) Fluorescence imaging system based on the monolithic DBR-integrated III-nitride LED chip.

DBR filter under an injected current of 400 mA, respectively. For the LED integrated with a DBR filter, only some light of longer wavelength can go through the DBR filter and is absorbed by the PCB packaging, resulting in the increase of green exciting light from the top side. The two sides of the LED chip are optically isolated by the PCB packaging and fiber housing, with an opening on the PCB used for coupling the backside light into a 200 μm diameter multimode fiber. The

coupled light is finally fed to an Ocean Optics HR4000 spectrometer for characterization, and the results are shown in Figure 3d. For the LED chip without a DBR filter, the backside EL spectra are the same as those of a normal green LED. For the LED chip with a DBR filter, the EL spectra indicate that most of the emitting light is rejected by the DBR filter, which is also verified by the optical microscopic images in the two left insets. Compared to the calculated EL intensity with a DBR filter, the measured curve in the right inset has a peak value at the green wavelength, which is caused by weak light leakage. Here, the calculated results are obtained by multiplying the EL intensity without a DBR filter and the measured transmission presented in Figure 2b. The leakage light would induce fixed output bias for the sensor system and the calibration can be performed easily. For the practical applications, reduced light leakage can be realized using well-designed packaging and improving the minimum detection capability of fluorescence intensity.

To further investigate the spectral characteristics for the fluorescence detection system, a set of fluorescence samples of different mass ratio were prepared, in which red-emitting (Sr, Ca) $AlSiN_3$:Eu^{2+} phosphors are adopted to mix uniformly with epoxy adhesive. The mass ratio is defined as the ratio of phosphor mass to total sample mass. Figure 4a illustrates the measurement setup. When the light of 528 nm peak wavelength emitting from the LED active layer illuminates the fluorescence sample, red fluorescent light is excited. Due to the specific wavelength selectivity of the DBR filter, most of the excitation green light is reflected by the filter and upward-propagating fluorescent red light can go through the filter. Finally, the fluorescent light can be coupled to the fiber and fed to an Ocean Optics HR4000 spectrometer for spectral analysis. Figure 4b shows the normalized EL intensity of the system with the DBR-integrated LED and fluorescence sample 1 (mass ratio 1:2). As the emission intensity of the LED increases with the injected current, the results indicate that the intensity of the fluorescent light increases with the excitation green light. Moreover, the peak value in the red range is much higher than the sub-peak value in the green range, with ratios larger than 21. Therefore, the influence of green light leakage can be neglected, and the fluorescent red light is dominant when the fluorescence detection system is used for sensing and imaging applications. Figure 4c,d shows the normalized EL intensity of the fluorescence detection system under different fluorescence samples using the LED without and with the DBR filter, respectively. We can see that the fluorescent light is relatively weak compared with the excitation green light if the LED without a DBR filter is adopted and it is hard to distinguish the fluorescence signal. For the system using the LED with a DBR filter, the intensity of dominant fluorescent red light increases with the mass ratio of fluorescence samples and the sub-peak value does not change with the mass ratio. We can infer that the green light leakage is mainly caused by the packaging instead of the DBR filter. Therefore, the green light leakage can be further depressed by optimizing the packaging if the system needs it.

By pasting the backside of the DBR-integrated III-nitride LED chip on to a silicon photodiode with a wide response range from 360 to 1100 nm, a simple and compact fluorescence sensor as shown in the inset of Figure 5a was developed to detect the fluorescence intensity. An aluminum PCB with an opening in the center was used for wire bonding and light isolation. Figure 5a shows the detected short-circuit

current of PD with respect to the injection current on the LED. The results are obtained by four measurements, in which the average values (denoted by the scattered data symbols) and standard deviations (denoted by the error bars) are both presented. It is clear that the detected current increases linearly with injected current. Therefore, the sensitivity can be improved by increasing the injected current with negligible effect on the standard deviations and measurement stability. Figure 5b shows the detected PD current with respect to the mass ratio of the fluorescent powder to the sample. The error bars are in line style and the thickness indicates the standard deviation. The results indicate that a large mass ratio leads to more fluorescence intensity, and therefore a larger detected PD current. For the mass ratio equal to zero, the detected current is mainly caused by green light leakage. By subtracting the background current, the fluorescence-induced light can be obtained, and we can deduce the fluorescence intensity utilizing the proposed sensor system. The total power consumption of the DBR-integrated LED chip is approximately 134 mW under 60 mA injection current. Furthermore, a fluorescence imaging system based on the monolithic DBR-integrated III-nitride LED chip is demonstrated in Figure 5c. The characters "NJUPT" are made by filling the red-emitting (Sr, Ca) $AlSiN_3$:Eu^{2+} phosphors into a glass mold. The red fluorescence characteristics can be observed clearly in the CCD system. When the phosphor is replaced by a white powder without fluorescence, the characters are invisible under green light illumination (see the Supporting Information, Video S1). By comparison, we can infer that the character imaging is only formed by the red fluorescent light but not the excitation green light. Hence, the fluorescence imaging system using the proposed monolithic DBR-integrated III-nitride LED chip can effectively avoid interference from excitation light and much reduce the total system size.

4. CONCLUSIONS

We have proposed a compact and reliable fluorescence detection system in which the DBR filter is directly grown on the backside of a III-nitride LED chip. The integrated DBR filter not only improves the LED light extraction on the front side but also realizes effective separation of excitation and fluorescent lights. Furthermore, the detection system allows for a removable sample unit and the requirement on sample preparation is much lower. The applications of the proposed detection system for fluorescence sensing and imaging have been successfully demonstrated and show great potential in portable systems.

■ ASSOCIATED CONTENT

Ⓢ Supporting Information

The Supporting Information is available free of charge at https://pubs.acs.org/doi/10.1021/acsomega.2c06839.

Validation of fluorescence imaging (MP4)

■ AUTHOR INFORMATION

Corresponding Authors

Jiabin Yan − *Grünberg Research Centre, Nanjing University of Posts and Telecommunications, Nanjing 210003, China*; ⓞ orcid.org/0000-0003-2460-5832; Email: jbyan@njupt.edu.cn

Xumin Gao − *Grünberg Research Centre, Nanjing University of Posts and Telecommunications, Nanjing 210003, China*; Email: gaoxm@njupt.edu.cn

Yongjin Wang − *Grünberg Research Centre, Nanjing University of Posts and Telecommunications, Nanjing 210003, China*; orcid.org/0000-0001-8109-4640; Email: wangyj@njupt.edu.cn

Authors

Jianwei Fu − *Grünberg Research Centre, Nanjing University of Posts and Telecommunications, Nanjing 210003, China*

Fan Shi − *Grünberg Research Centre, Nanjing University of Posts and Telecommunications, Nanjing 210003, China*

Feifei Qin − *Grünberg Research Centre, Nanjing University of Posts and Telecommunications, Nanjing 210003, China*

Pengzhan Liu − *Grünberg Research Centre, Nanjing University of Posts and Telecommunications, Nanjing 210003, China*

Complete contact information is available at:
https://pubs.acs.org/10.1021/acsomega.2c06839

Author Contributions

[†]J.Y., J.F., and F.S. contributed equally. J.Y. conceived and designed the experiments, performed the experiments, analyzed the data, and wrote the paper. X.G. designed and fabricated the chips. J.F., F.S., and P.L. performed the experiments. F.Q. analyzed the data. Y.W. proposed and coordinated the overall project. All authors reviewed the manuscript.

Notes

The authors declare no competing financial interest.

ABBREVIATIONS

GaN, gallium nitride; LED, light-emitting diode; LD, laser diode; PD, photodetector; DBR, distributed Bragg reflector; CCD, charge-coupled device; MQW, multiple quantum well; EL, electroluminescence; ICP, inductively coupled plasma; ITO, transparent indium tin oxide; PCB, printed circuit board

REFERENCES

(1) Tan, W.; Parpura, V.; Haydon, P. G.; Yeung, E. S. Neurotransmitter imaging in living cells based on native fluorescence detection. *Anal. Chem.* **1995**, *67*, 2575−2579.

(2) Demchenko, A. P. The future of fluorescence sensor arrays. *Trends Biotechnol.* **2005**, *23*, 456−460.

(3) You, Q. H.; Chan, P. S.; Chan, W. H.; Hau, S. C. K.; Lee, A. W. M.; Mak, N. K.; Mak, T. C. W.; Wong, R. N. S. A quinolinyl antipyrine based fluorescence sensor for Zn^{2+} and its application in bioimaging. *RSC Adv.* **2012**, *2*, 11078−11083.

(4) Liu, H.; Dong, Y. S.; Zhang, B. B.; Liu, F.; Tan, C. Y.; Tan, Y.; Jiang, Y. An efficient quinoline-based fluorescence sensor for zinc (II) and its application in live-cell imaging. *Sens. Actuators, B* **2016**, *234*, 616−624.

(5) Gupta, N. Spectropolarimetric imaging of laser-induced fluorescence. *IEEE Sens. J.* **2010**, *10*, 503−508.

(6) Yang, Z. M.; Mo, Q. Y.; He, J. M.; Mo, D. L.; Li, J.; Chen, H.; Zhao, S. L.; Qin, J. K. Mitochondrial-targeted and near-infrared fluorescence probe for bioimaging and evaluating monoamine oxidase a activity in hepatic fibrosis. *ACS Sens.* **2020**, *5*, 943−951.

(7) Tümay, S. O.; Haddad Irani-nezhad, M. H.; Khataee, A. Design of novel anthracene-based fluorescence sensor for sensitive and selective determination of iron in real samples. *J. Photochem. Photobiol., A* **2020**, *402*, 112819.

(8) Ezeh, V. C.; Harrop, T. C. A sensitive and selective fluorescence sensor for the detection of Arsenic (III) in organic media. *Inorg. Chem.* **2012**, *51*, 1213−1215.

(9) Borase, P. N.; Thale, P. B.; Shankarling, G. S. Dihydro-quinazolinone based "turn-off" fluorescence sensor for detection of Cu^{2+} ions. *Dyes Pigments* **2016**, *134*, 276−284.

(10) Brandl, M.; Posnicek, T.; Preuer, R.; Weigelhofer, G. A portable sensor system for measurement of fluorescence indices of water samples. *IEEE Sens. J.* **2020**, *20*, 9132−9139.

(11) Liu, T.; Wang, W.; Ding, H.; Yi, D. Smartphone-based hand-held optical fiber fluorescence sensor for on-site pH detection. *IEEE Sens. J.* **2019**, *19*, 9441−9446.

(12) Jewell, M. P.; Greer, M. D.; Dailey, A. L.; Cash, K. J. Triplet-triplet annihilation upconversion based nanosensors for fluorescence detection of potassium. *ACS Sens.* **2020**, *5*, 474−480.

(13) Pal, S.; Yonghang Shen, Y. H.; Mandal, J.; Tong Sun, T.; Grattan, K. T. V. Simultaneous measurement of strain (to 2000 $\mu\varepsilon$) and temperature (to 600 °C) using a combined Sb-Er-Ge-codoped fiber-fluorescence and grating-based technique. *IEEE Sens. J.* **2005**, *5*, 1462−1468.

(14) Lefèvre, F.; Chalifour, A.; Yu, L.; Chodavarapu, V.; Juneau, P.; Izquierdo, R. Algal fluorescence sensor integrated into a microfluidic chip for water pollutant detection. *Lab Chip* **2012**, *12*, 787−793.

(15) Novak, L.; Neuzil, P.; Pipper, J.; Zhang, Y.; Lee, S. An integrated fluorescence detection system for lab-on-a-chip applications. *Lab Chip* **2007**, *7*, 27−29.

(16) Chu, C. S.; Lin, K. Z.; Tang, Y. H. A new optical sensor for sensing oxygen based on phase shift detection. *Sens. Actuators, B* **2016**, *223*, 606−612.

(17) Pajuelo-Corral, O.; Rodríguez-Diéguez, A.; Beobide, G.; Pérez-Yáñez, S.; García, J. A.; San Sebastian, E. S.; Seco, J. M.; Cepeda, J. Alkaline-earth and aminonicotinate based coordination polymers with combined fluorescence/long-lasting phosphorescence and metal ion sensing response. *J. Mater. Chem. C* **2019**, *7*, 6997−7012.

(18) Suárez, P. L.; García-Cortés, M.; Fernández-Argüelles, M. T.; Encinar, J. R.; Valledor, M.; Ferrero, F. J.; Campo, J. C.; Costa-Fernández, J. M. Functionalized phosphorescent nanoparticles in (bio) chemical sensing and imaging - A review. *Anal. Chim. Acta* **2019**, *1046*, 16−31.

(19) Ryu, G.; Huang, J. S.; Hofmann, O.; Walshe, C. A.; Sze, J. Y. Y.; McClean, G. D.; Mosley, A.; Rattle, S. J.; deMello, J. C.; deMello, A. J.; Bradley, D. D. C. Highly sensitive fluorescence detection system for microfluidic lab-on-a-chip. *Lab Chip* **2011**, *11*, 1664−1670.

(20) Thrush, E.; Levi, O.; Ha, W.; Wang, K.; Smith, S. J.; Harris, J. S. Integrated bio-fluorescence sensor. *J. Chromatogr. A* **2003**, *1013*, 103−110.

(21) Thrush, E.; Levi, O.; Cook, L. J.; Deich, J.; Kurtz, A.; Smith, S. J.; Moerner, W. E.; Harris, J. S. Monolithically integrated semiconductor fluorescence sensor for microfluidic applications. *Sens. Actuators, B* **2005**, *105*, 393−399.

(22) Mukai, T. Recent progress in group-III nitride light-emitting diodes. *IEEE J. Sel. Top. Quant.* **2002**, *8*, 264−270.

(23) Chen, G.; Craven, M.; Kim, A.; Munkholm, A.; Watanabe, S.; Camras, M.; Götz, W.; Steranka, F. Performance of high-power III-nitride light emitting di-odes. *Phys. Status Solidi A* **2008**, *205*, 1086−1092.

(24) Li, K. H.; Fu, W. Y.; Choi, H. W. Chip-scale GaN Integration. *Prog. Quant. Electron.* **2020**, *70*, 100247.

(25) Wang, Q.; Yuan, G. D.; Liu, W. Q.; Zhao, S.; Zhang, L.; Liu, Z. Q.; Wang, J. X.; Li, J. M. Monolithic semi-polar (1101) InGaN/GaN near white light-emitting diodes on micro-striped Si (100) substrate. *Chin. Phys. B* **2019**, *28*, 087802.

(26) Mikulics, M.; Mayer, J.; Hardtdegen, H. H. Cutting-edge nano-LED technology. *J. Appl. Phys.* **2022**, *131*, 110903.

(27) Jiang, H. X.; Lin, J. Y. Nitride micro-LEDs and beyond - a decade progress review. *Opt. Express* **2013**, *21*, A475−A484.

(28) Mikulics, M.; Kordoš, P.; Gregušová, D.; Sofer, Z.; Winden, A.; Trellenkamp, S.; Moers, J.; Mayer, J.; Hardtdegen, H. Conditioning nano-LEDs in arrays by laser-micro-annealing: The key to their performance improvement. *Appl. Phys. Lett.* **2021**, *118*, 043101.